STRUCTURAL ANALYSIS OF HISTORICAL CONSTRUCTIONS
P. Roca, J.L. González, A.R. Marí and E. Oñate (Eds.)

STRUCTURAL ANALYSIS AND DURABILITY ASSESSMENT OF HISTORICAL CONSTRUCTIONS USING A FINITE ELEMENT DAMAGE MODEL

E. Oñate[1], A. Hanganu[1], A. Barbat[1], S. Oller[1], R. Vitaliani[2], A. Saetta [3] and R. Scotta[2]

[1]*E.T.S. Ing. de Caminos, Canales y Puertos*
Universidad Politécnica de Cataluña
08034 Barcelona
Spain

[2]*Ist. di Scienza e Técncia delle Construzioni*
Università di Padova
Padova
Italy

[3]*Dipartamento di Contruzioni dell'Architettura*
IUAV
Venezia
Italy

1. INTRODUCTION

Nowadays there is a general concern for preservation of historical constructions [1-3]. This will invariably require to pay greater attention to the reliable assessment of the structural conditions of the monuments and to the correct design of intervention measures. It is obvious that as time goes on, the number of historical constructions increases. In particular, many existing bridges, towers and dams as well as some relevant buildings can now be considered in every respect historical constructions [3].

The philosophy of conservation has the goal to preserve the original architectural message of any monument. The first step to reach such objective is the accurate prediction of the actual safety level of the structure. This includes the knowledge of both the mechanism of deterioration of the material and of the structural components and the evolution of degradation with time. The causes of deterioration usually can be subdivided in two main groups : physical-chemical-biological aggressive agents and mechanical problems. The latter can be nowadays accurately studied by means of coupled numerical- experimental procedures, where the structural behaviour is analyzed by advanced non-linear finite element models which are adequately calibrated using experimental data [5-28]. On the other hand, the analysis of the physical-chemical-biological deterioration requires the definition of "ad hoc" physical and numerical models for solving the equations of diffusion and transport of the aggressive species in order to predict the evolution of degradation phenomena due to different external agents [4,29-31].

The objective of this paper is to describe a methodology which can be effectively used for assessing the structural conditions and durability of historical masonry and concrete constructions. This includes the prediction of local and global behaviour up to structural failure under static and dynamic conditions. The approach combines the use of the concept of *damage* to represent the non-linear deterioration process of the material with advanced finite element models (including physical-chemical-biological degradation) and extensive experimental testing to calibrate and validate the overall numerical model.

The content of the paper is the following. In the next section a brief historical background of damage models is presented. Then the basic ingredients of the damage model used are described together with its implementation for finite element analysis of historical constructions. Finally, examples of preliminary applications of the model to the analysis of the central dome of St. Marks Basilica in Venice are presented.

2. BRIEF REVIEW OF CONSTITUTIVE MODELS FOR NON LINEAR ANALYSIS OF CONCRETE AND MASONRY STRUCTURES

Extensive experimental studies have been undertaken to characterize the response and ultimate strength of masonry and plain concrete under multi-axial stress states [6-8]. Considerable scatter of results has been observed and collaborative studies have been undertaken to identify the principal factors influencing this variation [7,11]. Several approaches, based on experimental data, have been used to represent the constitutive relationship under multi-axial stresses and these can be categorized into the five following groups: (a) linear and non linear elasticity theories, (b) perfect and work-hardening plasticity theories, (c) endochronic theory of plasticity, (d) plastic fracturing theory and damage theory.

A simple and popular model for non linear finite element analysis of concrete and masonry structures assumes elasto-plastic (or viscoplastic) constitutive equations for compression behaviour, whereas a conceptually more simple smeared elasto-brittle model is used for defining onset and progression of cracks at points in tension. Different versions of this model have been successfully used for non-linear analysis of masonry as well as plain and reinforced concrete structures [3,10,11,24]. A summary of some of the more recent contributions in each of those theories can be found in [6,10,11].

The elasto-plastic-brittle smeared model, in spite of its popularity, presents various controversial features such as the need for defining uncoupled behaviour along each principal stress (or strain) directions: the use of a shear retention factor to ensure some shear resistance along the crack; the lack

of equilibrium at the cracking point when more than one crack is formed: the difficulties in defining stress paths following the opening and closing of cracks under cycling loading conditions and the difficulty for dealing with the combined effect of cracking and plasticity at the damaged points [24].

It is well known that micro-cracking in concrete and masonry takes place at low load levels due to physical debonding between aggregate and mortar particles, or to simple micro-cracking in the mortar area. Cracking progresses following a non homogeneous path which combines the two mentioned mechanisms with growth and linking between micro-cracks along different directions. Experiments carried out on mortar specimens show that the distribution of micro-cracking is fairly discontinuous with arbitrary orientations [6]. This fact is supported by many experiments which show that cracking can be considered at microscopic level as a non directional phenomenon and that the propagation of micro-cracks follows an erratic path which depends on the size of the aggregate particles. Thus, the dominant cracking directions can be interpreted at macroscopic level as the locus of trajectories of the damage points (Figure 1).

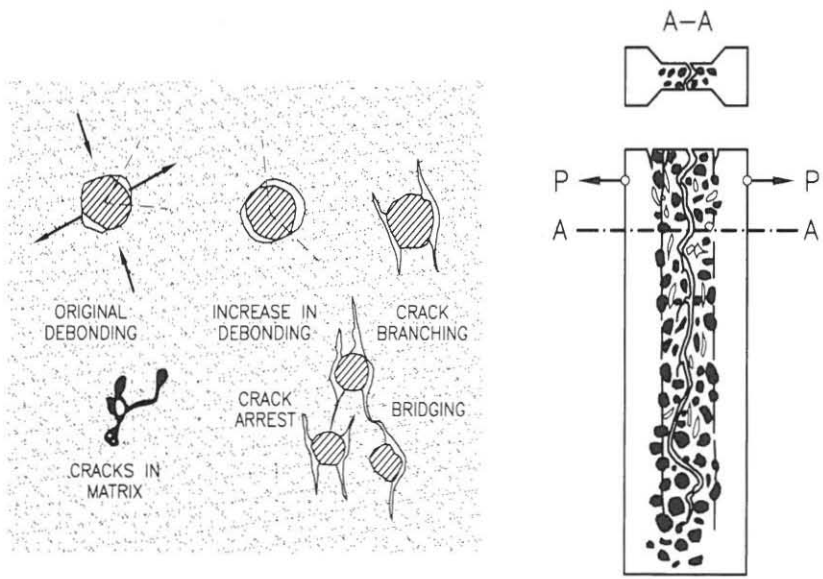

Figure 1. Mechanics of damage and propagation of a macroscopic crack in plain concrete

The above concepts support the idea that *the non linear behaviour of concrete and masonry can be modeled using concepts of damage theory only*

[10, 12, 13, 17-21] provided an adequate damage function is defined for taking into account the different response of concrete under tension and compression states. Cracking can, therefore, be interpreted as a *local damage effect*, defined by the evolution of known material parameters and by one or several functions which control the onset and evolution of damage.

One of the advantages of such a model is the independence of the analysis with respect to cracking directions which can be simply identified *a posteriori* once the non-linear solution is obtained [10,12,13]. This allows to overcome the problems associated to most elastic-plastic-brittle smeared cracking models. In this paper a model developed in recent years by the authors group [10-16,22-28] for non-linear analysis of concrete based on the concepts of *damage* mentioned above is extended for structural analysis of historical constructions. The model takes into account all the important aspects which should be considered in the non-linear analysis of concrete and masonry structures such as the different response under tension and compression, the effect of stiffness degradation due to mechanical and physical-chemical-biological effects and the problem of objectivity of the results with respect to the finite element mesh.

3. THE CONCEPT OF DAMAGE VARIABLE

In order to clarify the concept of damage consider a surface element in a damaged material volume. This surface has an area large enough to contain a representative number of defects, but still enabling to be referred as pertaining to a particular material point. Thus, if S_n denotes the overall section and $\bar{S}_n$ the effective resisting area ($S_n - \bar{S}_n$ is the area occupied by the voids), the *damage variable* d_n associated to this surface is (Figure 2)

$$d_n = \frac{S_n - \bar{S}_n}{S_n} = 1 - \frac{\bar{S}_n}{S_n} \tag{1}$$

Clearly, d_n represents the surface density of material defects and it will have a zero value when the material is in the undamaged virgin state. Conversely, the reduction of the effective resisting area will lead to an increase of damage until rupture defined by some critical value of d_n (bounded by the unreachable value of $d_n = 1$). Note that this is a directional definition of damage. In many cases a single scalar representation of damage is adopted (i.e. $d_n = d$) which suffices to ensure realistic material model [13,17-22]. It is worth noting, that in this case cracks at a microscopic point need not to have not particular direction and a macroscopic crack is then defined as the locus of damage points as previously mentioned.

An useful concept for understanding the effect of damage is that of

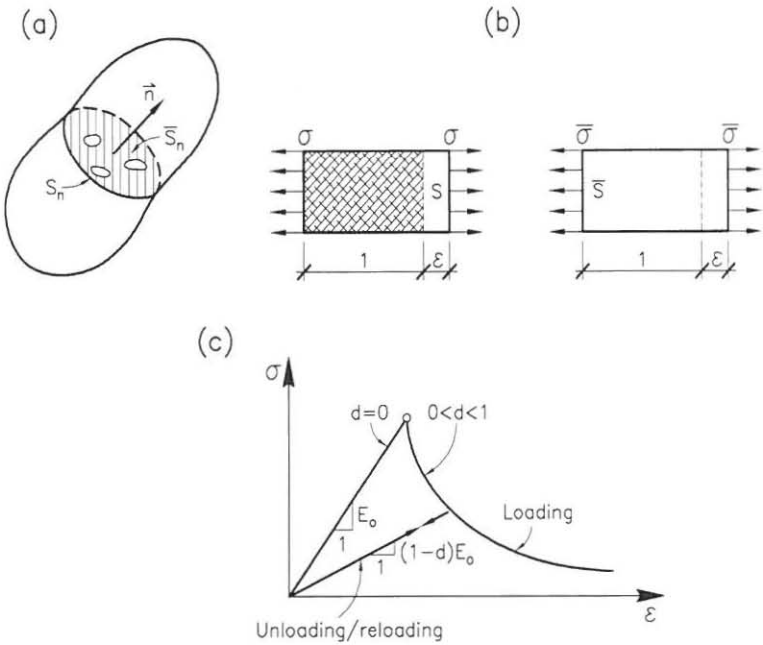

Figure 2. (a) Damaged surface; (b) Cauchy stress σ and effective stress $\bar{\sigma}$; (c) Evolution of uniaxial stress-strain curve

effective stress. The equilibrium relationship between the standard Cauchy stress σ and the "effective" stress, $\bar{\sigma}$, in the damaged bar specimen of Figure 2 is

$$\sigma S = \bar{\sigma}\bar{S} \tag{2}$$

and from (1) and (2)

$$\sigma = (1-d)\bar{\sigma} = (1-d)E\varepsilon \tag{3}$$

Clearly when a damaging process is occurring, the external loading is resisted by the effective stress area and, therefore, $\bar{\sigma}$ is a more physically representative parameter than σ (Figure 2).

4. CONTINUUM DAMAGE MODEL FOR MASONRY AND CONCRETE UNDER PHYSICAL, CHEMICAL AND BIOLOGICAL EFFECTS

4.1 Basic assumptions

As mentioned above, the deterioration mechanisms that occur in many concrete masonry structures can be divided in physical-chemical-biological causes and mechanical ones. The latter are usually due to an excess of stress acting on the material and can be studied by means of a standard damage model as explained previously. The physical-chemical-biological causes of degradations are due to the interaction between the environment and the building material. Here the presence of water plays a primary role. The main causes of degradations are listed in Table I [29-32,34].

Table 1 Classification of physical, chemical and biological degradation causes [34].

Type	Description of the sources of degradation
1. physical causes	1.1 freezing-thawing 1.2 leaching out 1.3 crystalisation of soluble salts
2. chemical causes	2.1 reaction between sulphate and hydrate calcium silicates with production of ettringite 2.2 reaction between sulphate and hydrate aluminates with production of thaumasite 2.3 reaction between calcium chloride and calcium hydroxide with production of hydrated calcium oxychloride 2.4 alkali-aggregate reaction
3. biological causes	3.1 formation of algae, lichens and fungi

4.1.1 *Field equations for environmental variables*

The differential equations governing moisture, heat and aggressive species flows in a porous material (such as masonry and concrete) in the hypothesis of existence of chemical reactions and by considering both diffusion and transport mechanisms can be written as

$$\begin{aligned}
\frac{\partial h}{\partial t} &= \nabla^{\mathrm{T}} c \nabla h + \frac{\partial h_s}{\partial t} + K \frac{\partial T}{\partial t} + \frac{\partial h_c}{\partial t} \\
\rho c_q \frac{\partial T}{\partial t} &= \nabla^{\mathrm{T}} b \nabla T + \frac{\partial Q_h}{\partial t} + \frac{\partial T_c}{\partial t} \\
\frac{\partial c}{\partial t} &= \nabla^{\mathrm{T}} D_c \nabla c + \frac{c}{\alpha} \frac{\partial w}{\partial t} + \frac{\partial c_c}{\partial t}
\end{aligned} \tag{4}$$

where h, T and c are respectively the relative humidity content, the temperature and the diffusive species concentration (e.g. chloride, sulphate, CO_2, etc.) and w is the water content. Q_h is the outflow of heat per unit volume of solid, b is the thermal conductivity and $\partial(\cdot)_c/\partial t$ denotes changes due to the carbonation per time unit. A more precise definition of these symbols can be found in [29,30].

The diffusivities of relative humidity h and the aggressive species D_c are assumed to be strongly dependent on the pore humidity, temperature, degree of hydration of cement (that is the equivalent curing time) and the precipitate concentration c_f (if the product of the chemical reaction is a precipitate, like the calcium carbonate in the carbonation process). These latter two facts slow the diffusion phenomenon for long term results due to the reduction of the porosity. The (non linear) expressions of the diffusivities as a function of h, T and c can be found in [34]. Note that the mathematical form of the problem is similar to that of the corrosion problem of the steel in concrete and the freeze-thaw problem [29,30,33].

4.1.2 *Numerical solution of environmental variables*

Due to the complexity resulting from the non linearities occurring in the definition of the diffusivities and the coupling of the differential equations (4), analytical solutions are very difficult to obtain and a numerical approach should be preferred. There the finite element method seems to be the more adequate procedure to solve the space-time equations and it has been successfully used by the authors in this context [29,30,34].

Application of the well-known Galerkin procedure after space discreti-

sation leads to the following systems of equations of coupled ordinary differential equations in time

$$\begin{aligned} \frac{\partial \boldsymbol{h}}{\partial t} + \boldsymbol{C}_1 \boldsymbol{h} - \boldsymbol{K}\frac{\partial \boldsymbol{T}}{\partial t} - \frac{\partial \boldsymbol{h}_c}{\partial t} = 0 \\ \boldsymbol{C}_2\frac{\partial \boldsymbol{T}}{\partial t} + \boldsymbol{B}\boldsymbol{T} - \frac{\partial \boldsymbol{Q}_n}{\partial t} - \frac{\partial \boldsymbol{T}_c}{\partial t} = 0 \\ \frac{\partial \boldsymbol{C}}{\partial t} + \boldsymbol{D}\boldsymbol{C} - \boldsymbol{C}_3\frac{\partial \boldsymbol{w}}{\partial t} - \frac{\partial \boldsymbol{C}_c}{\partial t} = 0 \end{aligned} \tag{5}$$

where $\boldsymbol{h}$, $\boldsymbol{T}$ and $\boldsymbol{C}$ represent the discrete relative humidity content, the discrete temperature and the discrete diffusive species concentration vectors. For the detailed expressions of the matrices in (5) see [29,30,33].

The system (5) can be written in the following concise form

$$\boldsymbol{A}\dot{\boldsymbol{x}} + \boldsymbol{B}\boldsymbol{x} = \boldsymbol{q} \tag{6}$$

where the meaning of the terms in the eq. (6) follows immediately from eq. (5). The solution in time of eq. (6) can be easily attempted following a standard one step algorithm giving

$$\left[\frac{1}{\Delta t}\boldsymbol{A} + \alpha \boldsymbol{B}\right]\boldsymbol{x}^{n+1} = \boldsymbol{q}^n - \left[(1-\alpha)\boldsymbol{B} - \frac{1}{\Delta t}\boldsymbol{A}\right]\boldsymbol{x}^n \tag{7}$$

where $(\cdot)^n$ denotes values at time t^n, Δt is the time increment and α is a stability parameter [35]. The algebraic non linear equations (6) is thus solved by a direct approach. Details of the stability and convergence conditions in the solution of eq. (7) can be found in [33,35].

4.2 Coupling environmental and mechanical damage

The coupling of physical-chemical-biological effects with strength characteristics can be taken into account in the damage model by modifying eq.(3) as

$$\sigma = \beta(1-d)E\varepsilon \tag{8}$$

where β is a physical-chemical-biological (PCB) parameter such that $\beta_c < \beta \leq 1$. The value of β approaches the critical lower value β_c as the PCB degradation process reaches its maximum effect. Eq.(8) can be rewritten as

$$\sigma = (1-d^*)E\varepsilon \tag{9}$$

with $$d^* = 1 - \beta(1 - d) \tag{10}$$

Clearly the effect of β is that of reducing the mechanical strength. Note that as $\beta \longrightarrow \beta_c$ then $d^* \longrightarrow d$. The evolution of β depends on that of moisture, temperature and aggressive species within the (porous) material. The physical parameters in this diffusion process depend also on the overall degradation level through the damage variable d and the problem is thus fully coupled [33,34]. A full coupled analysis involves the finite element solution of the differential equations governing the transport of diffusing species together with those governing the structural behaviour. The PCB-mechanical coupling can be tackled by means of a staggered scheme [33,35]. Very few applications of the full coupled solutions can be found in the literature. Preliminary results for simple test problems have been recently reported in [33,34]. The analysis can be obviously simplified by choosing a fixed value of β, which is equivalent to accepting a certain level of PCB degradation at the time of analysis, or by defining an appropriate time evolution of the PCB parameters.

4.3. Three-dimensional model and evolution laws

Equation (8) can be extended to define the constitutive equation of a three dimensional specimen in vector form as

$$\boldsymbol{\sigma} = \beta(1 - d)\bar{\boldsymbol{\sigma}} = \beta(1 - d)\boldsymbol{D}\boldsymbol{\varepsilon} \tag{11}$$

where $\boldsymbol{D}$ is the elastic constitutive matrix $\boldsymbol{\sigma}$ and $\boldsymbol{\varepsilon}$ are the standard stress and strain vectors.

The model defined by eq. (11) requires the knowledge of the damage and PCB variables d and β ,respectively at every stage of the history of the construction. For this purpose one must define:

For the damage variable $\boldsymbol{d}$

a) A suitable scalar norm τ of the strain tensor (or alternatively of the undamaged stress tensor). Here, several possibilities exist and a suitable option for concrete and masonry is [10,23]

$$\tau = \left(\theta + \frac{1 - \theta}{n}\right)\left[\bar{\boldsymbol{\sigma}}^T \boldsymbol{D}^{-1} \bar{\boldsymbol{\sigma}}\right]^{1/2} \tag{12}$$

where $n = f'_c/f'_t$ is the ratio between the compression and tension limit strengths.

$$\theta = \frac{\sum_{i=1}^{3} <\bar{\sigma}_i>}{\sum_{i=1}^{3} |\bar{\sigma}_i|} \quad \text{with} <\pm\bar{\sigma}_i>= \frac{1}{2}(|\sigma_i| \pm \sigma_i) \tag{13}$$

Expression (13) accounts for the different limit behaviour of the material under compression and tension states.

b) A damage criterion formulated in the strain of the undamaged stress spaces. The simplest form of this can be written as

$$F(\tau, r) = \tau - r \leq 0 \tag{14}$$

where τ is the norm defined in (8) and r is the damage threshold value. Damage grows when the norm τ exceeds the current threshold value. In particular, damage is initiated when τ exceeds for the first time the value r° (typically $r^\circ = f_t'/\sqrt{E}$ is taken [10,13]).
Figure 3 shows the form of the limit surface $\tau^\circ - r^\circ$ defining the onset of damage for the expression of τ given by eq.(12).

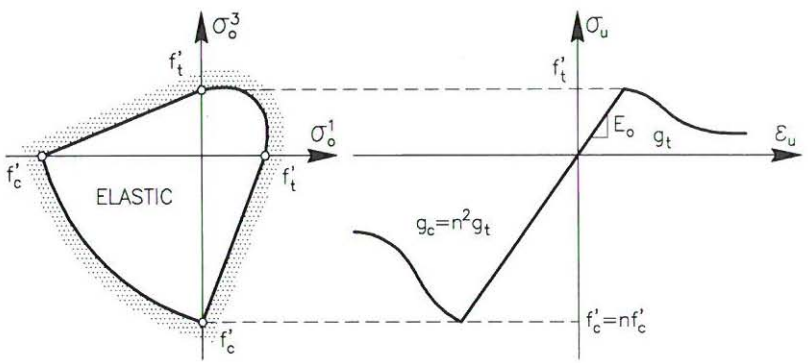

Figure 3. Limit damage surface and uniaxial stress-strain curve for the model of eq. (9)

c) Evolution laws for the damage variable d and the damage threshold value r. These can be written as [28], [31].

$$d = G(r) \quad , \quad r = \max\{r^\circ, \tau\} \tag{15}$$

where G is a suitable monotonic scalar function taken as

$$G(r) = 1 - \frac{r^\circ}{r} \exp\left\{A\left(1 - \frac{r}{r^\circ}\right)\right\} \tag{16}$$

Note that $G(r^\circ) = 0$ and $G(\infty) = 1$ as expected. The parameter A is determined from the energy dissipated in an uniaxial tension test as [10,23]

$$\frac{1}{A} = \frac{g_f E}{(f_t')^2} - \frac{1}{2} \tag{17}$$

where $g_f = G_f/l^*$, G_f being the specific fracture energy per unit area (taken as a material property), l^* is the characteristic length of the fractured domain. As always $g_f \geq (f_t')^2/2E$ (the material must dissipate at least the energy stored when the elastic limit is reached), parameter A must be positive [28]. Defining $g_f' = g_f - (f_t')^2/2E$, an alternative expression for (17) is

$$\frac{1}{A} = \frac{g_f' E}{(f_t')^2} \tag{17a}$$

For the PCB variable β:

a) A suitable scalar norm of the residual strength. Here the simplest option is to choose the same norm τ proposed for the damage variable.
b) An evolution law for the PCB variable β. This can be written following [33] as

$$\beta = F(\tau, c) \tag{18a}$$

with

$$F(\tau, c) = \gamma + (1 - \gamma)\left[1 + \left(\frac{2c}{c_{\text{ref}}}\right)^4\right]^{-1} \tag{18b}$$

where $\gamma = \frac{\tau}{\tau_{\text{ref}}}$ is the ratio between the actual strength norm τ and the residual strength norm, corresponding to $c = c_{\text{ref}}$, i.e. the reference concentration of the diffusing species (chloride, sulphate, CO_2, etc.) for which the PCB degradation process reaches its maximum effect.

The experimental characterization of the model requires the following material parameters : Young modulus and Poisson ratio, tension and compression limit strengths and specific fracture energy obtained from uniaxial tests as well as the time evolution of the concentration of the diffusing species obtained from separate solution of diffuse transport equations or by experimental measurements [29-34].

4.4. Finite element structural analysis

The damage model presented above is extremely simple in comparison with more sophisticated models for frictional materials. The finite element implementation follows the standard process [35]:

a) Finite element discretisation of the structure and interpolation of the displacement field within each element as :

$$\boldsymbol{u} = \boldsymbol{N}\boldsymbol{a} \tag{19}$$

where $\boldsymbol{u}$ is the displacement vector, $\boldsymbol{N}$ is the shape function matrix and $\boldsymbol{a}$ is the vector containing the displacements of the element nodes.

b) Discretisation of the strain and stress fields as

$$\boldsymbol{\varepsilon} = \boldsymbol{L}\boldsymbol{u} = \boldsymbol{L}\boldsymbol{N}\boldsymbol{a} = \boldsymbol{B}\boldsymbol{a} \tag{20}$$

$$\boldsymbol{\sigma} = \beta(1-d)\boldsymbol{D}\boldsymbol{\varepsilon} = \beta(1-d)\boldsymbol{D}\boldsymbol{B}\boldsymbol{a} \tag{21}$$

where $\boldsymbol{L}$ is the appropriate strain operator and $\boldsymbol{B}$ is the strain matrix.

c) Derivation of the (non-linear) discretised equations. Substituting equations (19)-(21) into the principle of virtual work [35]

$$\int_V \delta\boldsymbol{\varepsilon}^{\mathrm{T}}\boldsymbol{\sigma}\, dV = \int_V \delta\boldsymbol{u}^{\mathrm{T}}\boldsymbol{b}\, dV + \int_S \delta\boldsymbol{u}^{\mathrm{T}}\boldsymbol{t}\, dS \tag{22}$$

gives after standard algebra

$$\boldsymbol{\Psi} = \boldsymbol{p} - \boldsymbol{f} \tag{23}$$

$$\boldsymbol{p} = \int_V \boldsymbol{B}^{\mathrm{T}}\boldsymbol{\sigma}\, dV \tag{24}$$

$$\boldsymbol{f} = \int_V \boldsymbol{N}^{\mathrm{T}}\boldsymbol{b}\, dV + \int_S \boldsymbol{N}^{\mathrm{T}}\boldsymbol{t}\, dS \tag{25}$$

In the above equations $\boldsymbol{b}$ and $\boldsymbol{t}$ are body force and distributed force vectors respectively, $\delta\boldsymbol{\varepsilon}$ and $\delta\boldsymbol{u}$ denote the virtual strains and virtual displacements, respectively and $\boldsymbol{\Psi}$ is the so-called *residual force* vector which expresses the equilibrium between the external forces vector, $\boldsymbol{f}$ and the internal forces vector, $\boldsymbol{p}$.

The system of equations (23) is *non-linear* due to the dependence of the stresses on the damage and PCB parameters d and β through eq.(21). A summary of the main steps of the non-linear solution is shown in Box 1.

nth load increment, ith iteration

$$\boldsymbol{a}_i^n = \boldsymbol{a}^{n-1}$$

Compute displacement increment

$$\Delta \boldsymbol{a}_i^n = -[\boldsymbol{H}_i^n]^{-1} \boldsymbol{\Psi}_i^n$$

$\boldsymbol{\Psi}_i^n$: residual force vector $(= \int_V \boldsymbol{B}^{\mathrm{T}} \boldsymbol{\sigma}\, dV - \boldsymbol{f})$

$\boldsymbol{H}_i^n$: iteration matrix (i.e. tangent stiffness matrix)

Update displacements and strains

$$\boldsymbol{a}_{i+1}^n = \boldsymbol{a}_i^n + \Delta \boldsymbol{a}_i^n$$

$$\boldsymbol{\varepsilon}_{i+1}^n = \boldsymbol{\varepsilon}_i^n + \boldsymbol{B} \Delta \boldsymbol{a}_i^n$$

Evaluate stresses

(1) Compute undamaged stresses: $\bar{\boldsymbol{\sigma}}_{i+1}^n = \boldsymbol{D} \boldsymbol{\varepsilon}_{i+1}^n$

(2) Evaluate r_{i+1}^n using eq.(12): $r_{i+1}^n = \tau_{i+1}^n$

(3) Update r, d and β

$r_{i+1}^n = \max(r^{n-1}, r_{i+1}^n)$

$d_{i+1}^n = G(r_{i+1}^n)$

$\beta_{i+1}^n = F(\tau_{i+1}^n, c_{i+1}^n)$

(4) Update stresses: $\boldsymbol{\sigma}_{i+1}^n = (1 - d_{i+1}^n) \boldsymbol{\sigma}_{i+1}^n$

Evaluate residual force vector: $\boldsymbol{\Psi}_{i+1}^n$

Check convergence: $\|\boldsymbol{\Psi}_{i+1}^n\| \leq \epsilon \|\boldsymbol{f}\|$?

No: Continue iterations: $i = i + 1$

Yes: $\boldsymbol{a}^n = \boldsymbol{a}_{i+1}^n$

Next load increment: $n = n + 1$

Box 1. Quasi-static non linear finite element structural solution using the environmental-mechanical damage model

Note that the process is relatively simple as no special algorithm for integration of the constitutive equations is needed as the stresses are explicitly given by eq.(21). Further information including details of the consistent computation of the tangent constitutive matrix can be found in [28].

The concentration of diffusing PCB species, c, at each stage of the structural life should be determined by a separate transient solution of the PCB transport equations which in turn depend on the damage level as above explained. The solution of the full coupled problem in time is schematically shown in Box 2.

0. New time increment $t^{n+1} = t^n + \Delta t$

1. Solve evolution equation for c_i^{n+1}
   - $c_i^{n+1} = f(c_i^n, \boldsymbol{\sigma}^n, d^n, ...)$

2. Compute $\beta^{n+1} = \beta(c_i^{n+1})$

3. Solve structural problem at time t^{n+1}
   - Solve $\boldsymbol{p}(\boldsymbol{a}^{n+1}) - \boldsymbol{f}^{n+1} = 0$ for $\boldsymbol{a}^{n+1}$, $\boldsymbol{\varepsilon}^{n+1}$ and $\boldsymbol{\sigma}^{n+1}$ using
     - $\boldsymbol{\sigma}^{n+1} = \beta^{n+1}(1 - d^{n+1})\boldsymbol{\varepsilon}^{n+1}$

4. Repeat steps 1. to 3. until convergence of environmental and mechanical solutions at time t^{n+1}

5. Compute global damage index D^{n+1} at time t^{n+1}

6. Next time increment – go to step 0.

Box 2. Full coupled transient solution linking environmental and mechanical damage.

A simpler alternative is to assume an uncoupled behaviour between the mechanical and environmental damage parameters and to obtain an analytical expression of c by solving independently the transport equations for the diffusing species under different degradation assumptions [39]. The mechanical problem can thus be separately solved for a fixed value of β to obtain the structural response and failure load of the construction at any desired time of its history. This process is sketched in Box 3.

1. Uncoupled transient environmental damage analysis

1.1 Solve for the time evolution of c_i

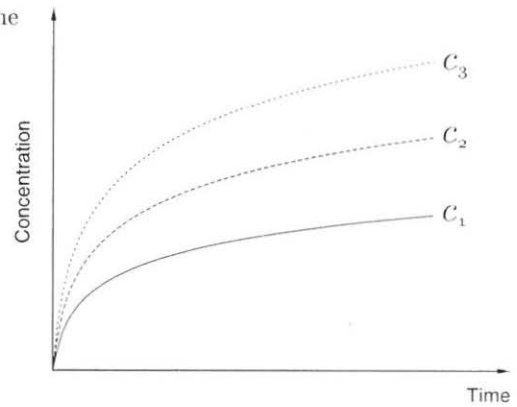

1.2 Compute $\beta(t)$

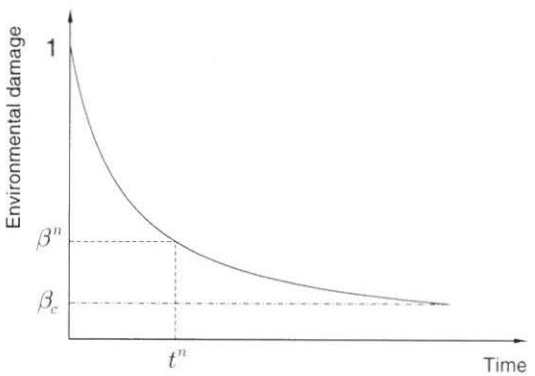

2. Perform quasi-static structural analysis at time $t = t^n$

- $\beta^n = \beta(t^n)$
- Solve $\boldsymbol{p}(\boldsymbol{a}^n) - \boldsymbol{f}^n = 0$ for $\boldsymbol{a}^n$, $\boldsymbol{\varepsilon}^n$ and $\boldsymbol{\sigma}^n$ using:
  - $\boldsymbol{\sigma}^n = \beta^n(1 - d^n)\boldsymbol{\varepsilon}^n$
- Compute global damage index D^n

Box 3. Quasi-static structural analysis using information from uncoupled transient environmental damage computations.

The *dynamic solution* under time dependent forces follows a similar pattern. Inclusion of dynamic effects in the virtual work equation (22) leads after discretisation to the well known transient equation system [35].

$$\boldsymbol{M}\ddot{\boldsymbol{a}} + \boldsymbol{C}\dot{\boldsymbol{a}} + \boldsymbol{K}\boldsymbol{a} = \boldsymbol{f}(t) \tag{26}$$

where $\dot{\boldsymbol{a}}$ and $\ddot{\boldsymbol{a}}$ are nodal velocity and acceleration vectors, respectively. $\boldsymbol{M}$ and $\boldsymbol{C}$ are the mass and damping matrices and $\boldsymbol{f}(t)$ is the time dependent nodal force vector.

A full non-linear transient solution of eq.(26) is now possible using standard time integration algorithms giving the displacements, velocities, accelerations, strains and stresses as well as the local and global damage indexes at each time of the deformation process. A detailed description of the dynamic finite element solution falls outside the scope of this paper. The interested reader can find full details in [28,35].

5. THE CONCEPT OF GLOBAL DAMAGE

The global strength of the structure can be assessed by means of a *global damage* index D. The simplest definition for D is the following

$$D = 1 - \frac{\bar{U}}{U} \tag{27}$$

where $\bar{U}$ and U are the internal energies corresponding to the damaged and undamaged states, i.e.

$$\begin{aligned} \bar{U} &= \boldsymbol{a}^T \int_V \boldsymbol{B}^T \boldsymbol{\sigma} dV = \boldsymbol{a}^T \int_V \boldsymbol{B}^T (1-d)\bar{\boldsymbol{\sigma}} dV \\ U &= \boldsymbol{a}^T \int_V \boldsymbol{B}^T \bar{\boldsymbol{\sigma}} dV \end{aligned} \tag{28}$$

In (28) the total energy of the structure is obtained by sum of the element contributions in the standard manner.

Note that global structural failure corresponds to a value of D approaching unity. Thus, the computation of the local and global damage indices provides a useful tool for monitoring in detail the evolution of the non linear response of the structure up to failure.

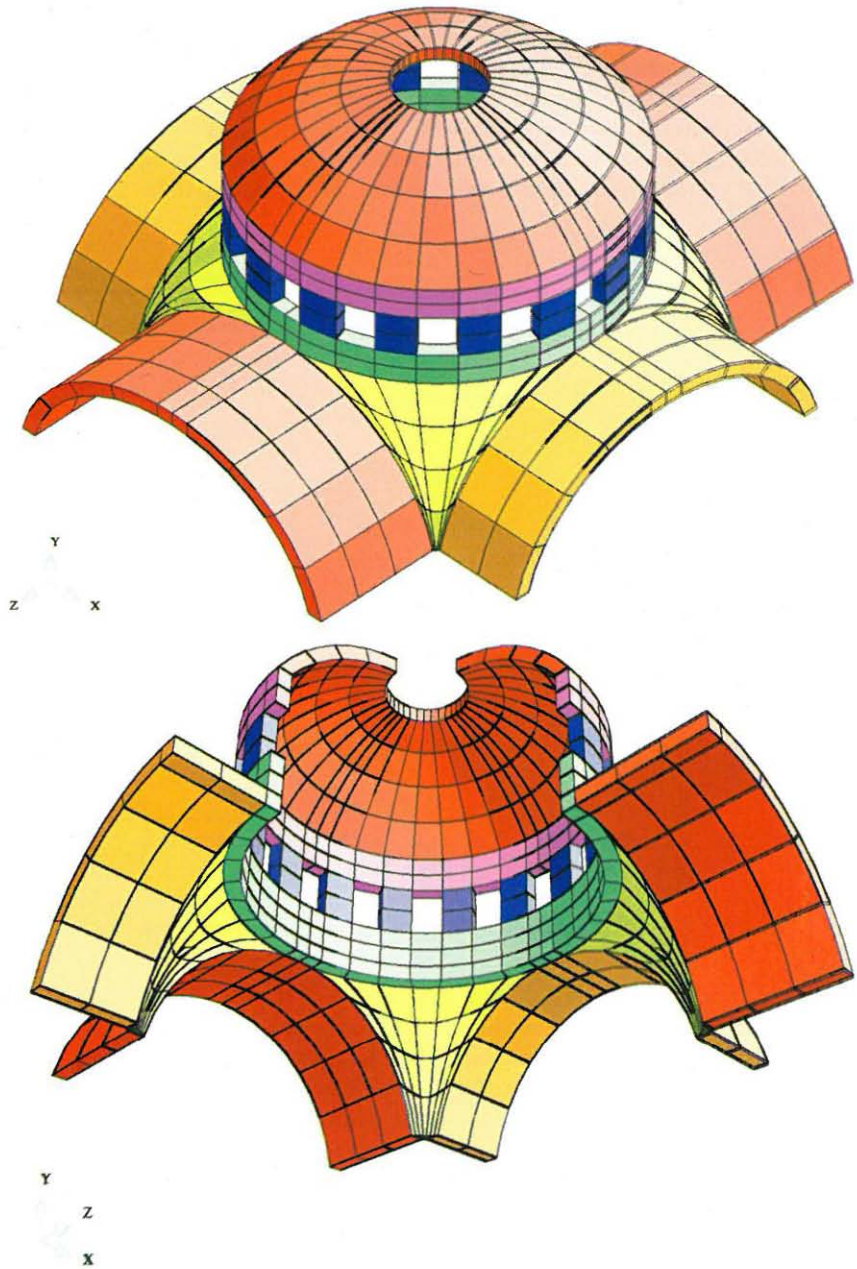

Figure 4. Views of the 3D finite element mesh of St. Marks Basilica Dome.

6. ANALYSIS OF ST. MARKS BASILICA IN VENICE

The methodology presented is currently being applied by the authors to analyze structural elements of St. Marks Basilica in Venice for which cracking patterns have been detected. The first example presented is the preliminary damage analysis of the central dome under various static and dynamic conditions using a finite element code developed by the authors [28].

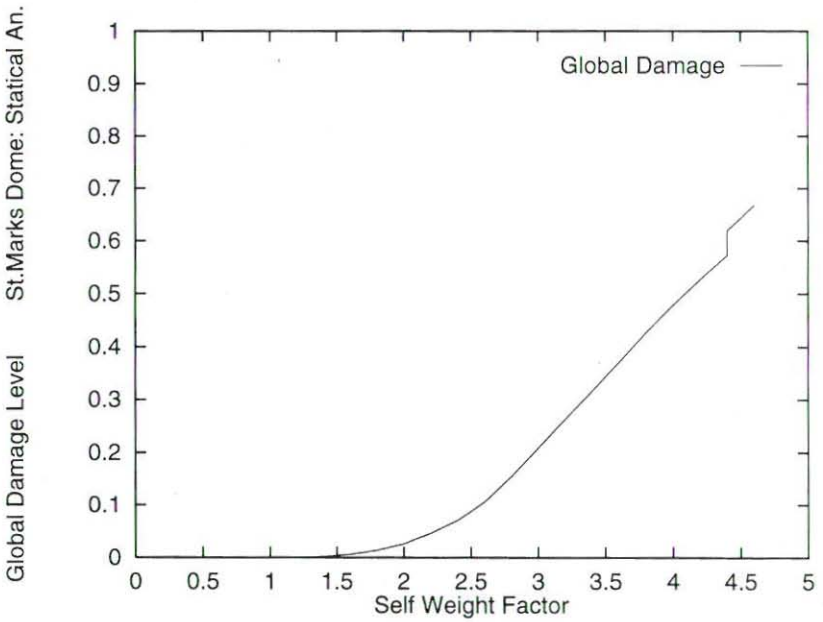

Figure 5. Global damage evolution for the static analysis.

Figure 4 shows different views of the finite element meshes of the structure using standard 20 node isoparametric hexahedral elements. All points at the base ($y = 0$) have the vertical displacement restricted. In addition the displacement in the plane $y = 0$ of two base points have been also restricted to avoid rigid body motions. The material properties assumed in the analysis are the following :

Case 1:

Stone

- E = 600.000 kg/cm^2, ν=0.15
- Tension limit strength = 40 kg/cm^2
- Compression limit strength = 400 kg/cm^2
- Density = 2.7 g/cm^3

Masonry (vertical cylindrical wall elements)

- E = 200.000 kg/cm^2, ν=0.15
- Tension limit strength = 10 kg/cm^2
- Compression limit strength = 100 kg/cm^2
- Density = 2.4 g/cm^3

The first solution attempted is the analysis of the limit static structural strength under self weight loading. The study has been undertaken for a constant value of the PCB parameter $\beta = 0.9$ for simplicity. Figure 5 shows the evolution of the global damage index D for increasing values of the self weight up to failure characterized by a value of D rapidly approaching unity. Convergence of the non-linear solution was lost for $D = 0.8$ and a safety coefficient of $\simeq 4.6$ was found. The evolution of the local damage index d contours is plotted in Figures 6a-c. Note that the maximum value of d reaches 0.9513 at the dome base where existing cracks have been observed in practice. The contours of equal vertical displacement and a picture of the deformed shape of the structure at the failure load are plotted in Fig.7.

The same analysis was repeated for reduced values of the masonry strength of

CASE 2

- Tension limit strength = 5 kg/cm^2
- Compression limit strength = 50 kg/cm^2

CASE 3

- Tension limit strength = 1 kg/cm^2
- Compression limit strength = 10 kg/cm^2

while keeping the rest of the material properties constant and equal to those chosen in Case 1.

Figure 8 shows the evolution of the safety coefficient for the three different cases studied. It is interesting to note that the safety coefficient does not substantially increase for values of the tension limit strength of the masonry greater than 5 kg/cm^2. This is due to the change of the deformation mode of the structure as the strength of the masonry wall increases which leads to accelerated failure of the stone arches, as expected.

The next study is the dynamic analysis of the structure under a hypothetic earthquake. The material parameters and boundary conditions coincide with those of Case 1 described above.

The analysis was performed in two steps. First, the static solution under

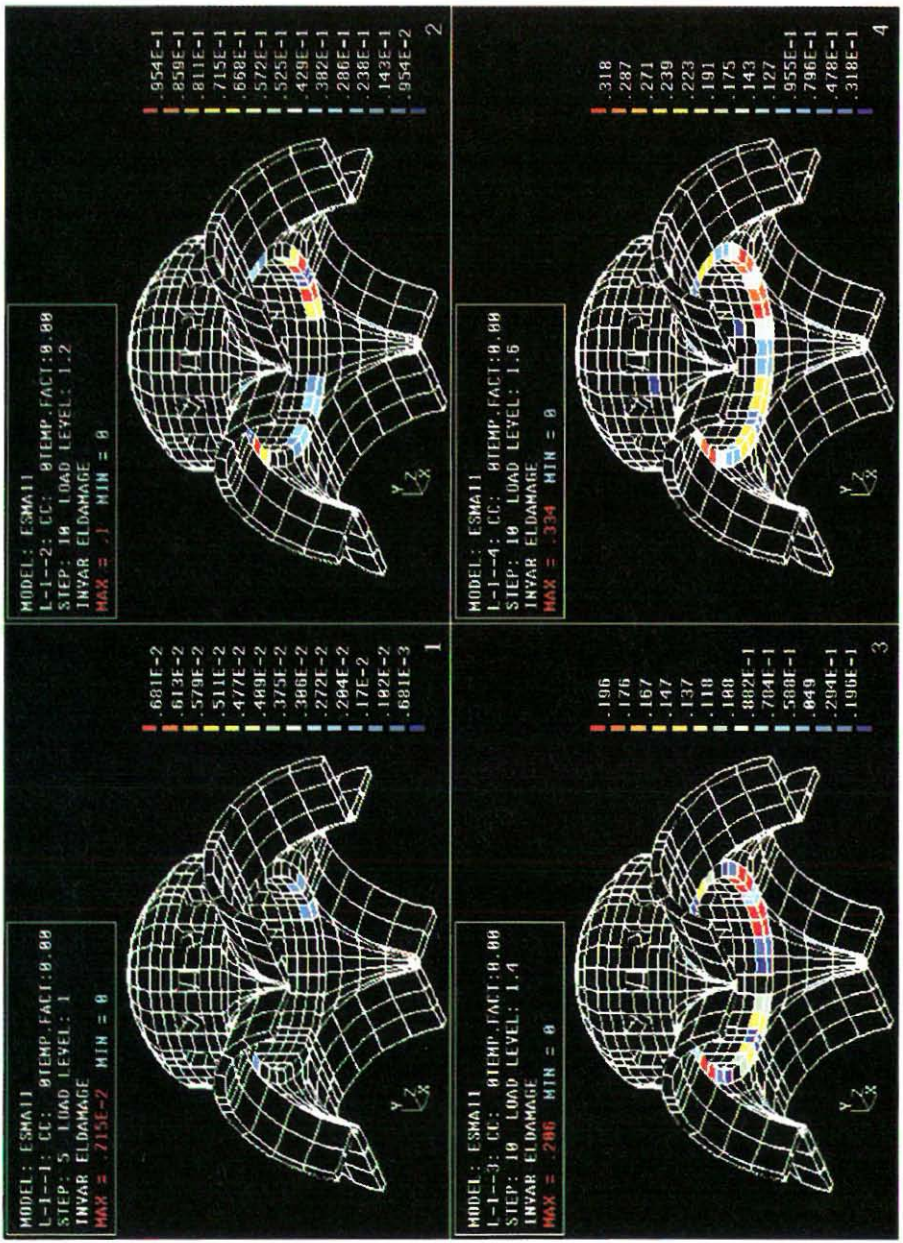

Figure 6.a Contours of the damaged zones for load factors of 1.0, 1.2, 1.4 and 1.6, respectively.

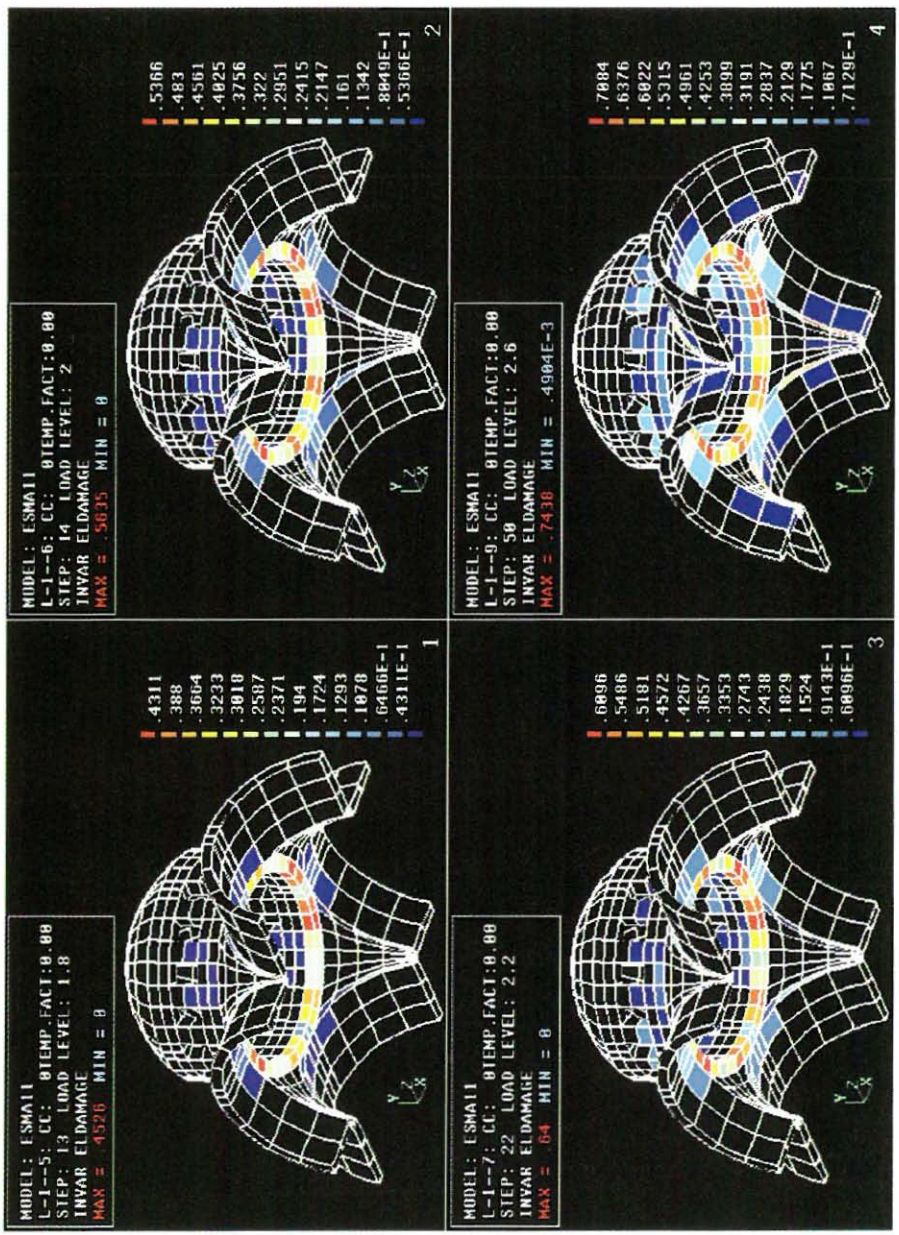

Figure 6.b Contours of the damaged zones for load factors of 1.8, 2.0, 2.2 and 2.6, respectively.

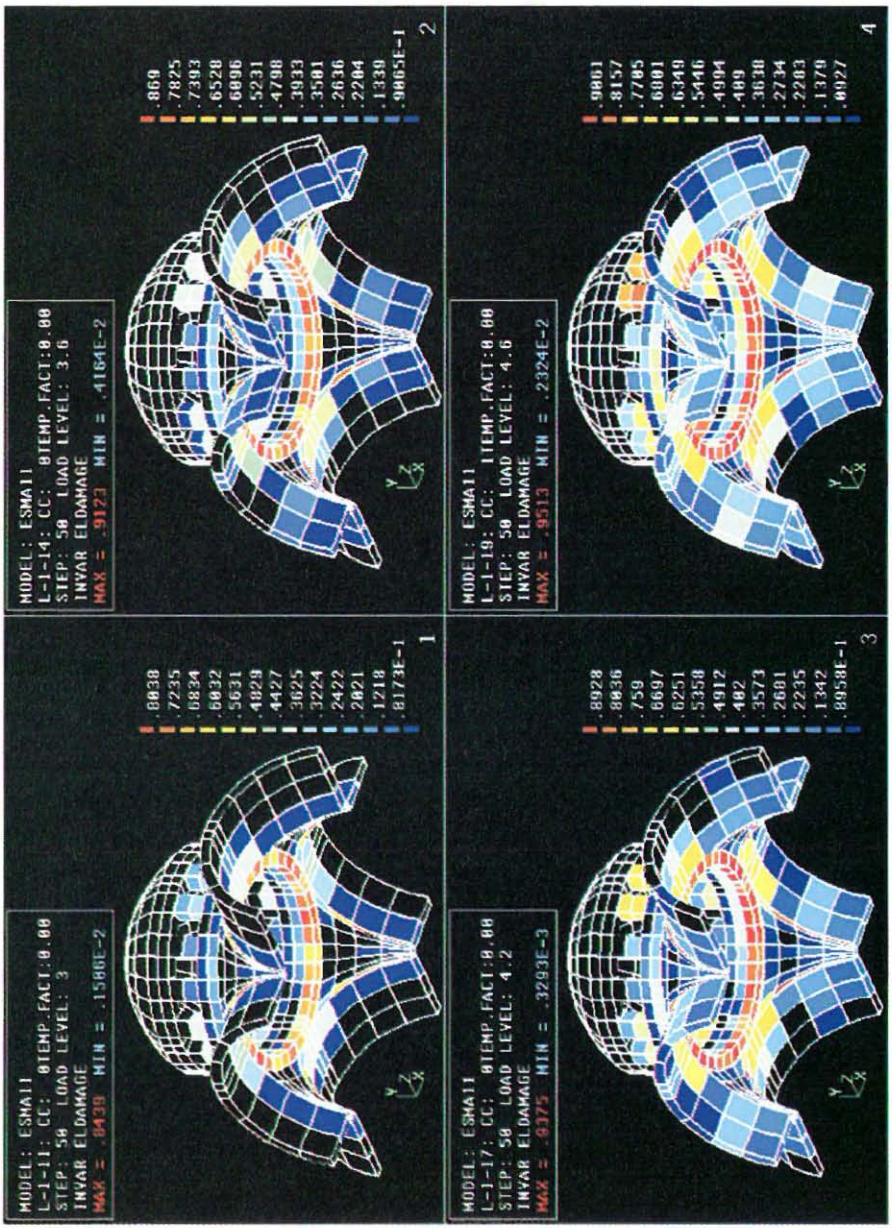

Figure 6.c Contours of the damaged zones for load factors of 3.0, 3.6, 4.2 and 4.6, respectively.

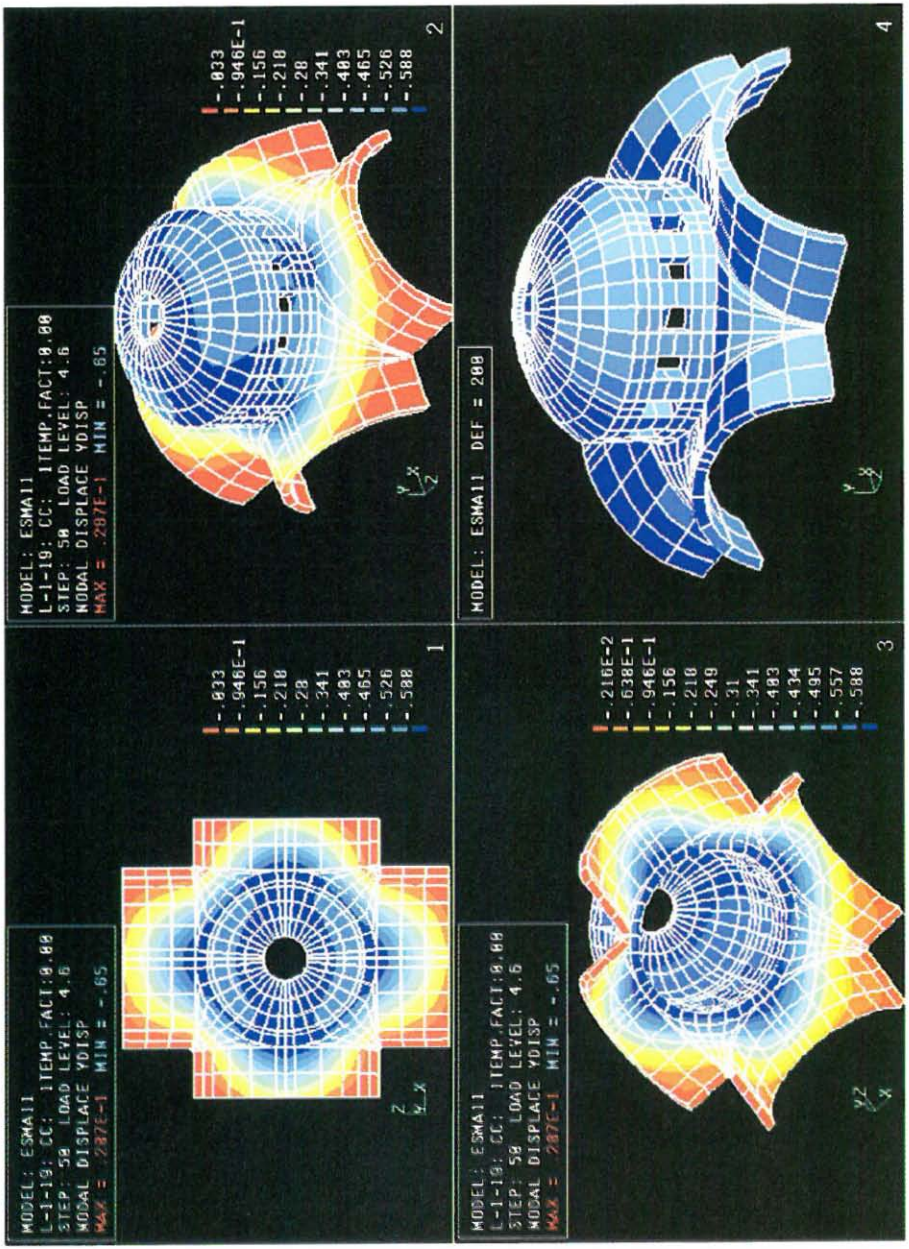

Figure 7. Contours of equal displacement and deformed shape at collapse.

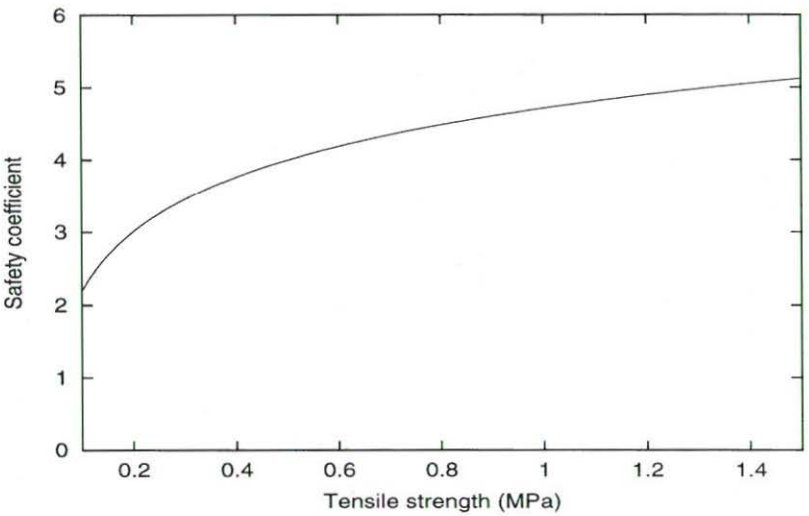

Figure 8. Safety coefficient evolution against the tensile strength of masonry.

self weight was obtained and next the synthetic acceleration shown in Figure 9 was applied to the base of the initially self-loaded structure. The evolution of the global damage index D with time is plotted in Figure 10. Note that global failure is obtained after 3.02 seconds. Failure occurs due to fracture of the masonry elements at the mid-hight of the cylindrical wall as clearly shown in Figures 11a-b. The deformed shapes of the structure at different times during the earthquake can be seen in Figure 12.

The last example corresponds to the full three-dimensional analysis of the five domes of St. Marks Basilica. Figure 13 shows the mesh of 7676 20-noded hexahedra involving 48505 nodes used for the analysis. 2265 15-noded triangular prisms were also used as transition elements in some zones. The material properties for the stone were taken the same as for the analysis of the single dome in the previous example. The properties for the cylindrical walls masonry where taken as:

- wall 1 E=30000kg/cm^2, ν=0.15, σ_c=40kg/cm^2, σ_t=10kg/cm^2
- wall 2 E=60700kg/cm^2, ν=0.15, σ_c=40kg/cm^2, σ_t=10kg/cm^2
- wall 3 E=250000kg/cm^2, ν=0.15, σ_c=300kg/cm^2, σ_t=30kg/cm^2
- wall 4 E=90000kg/cm^2, ν=0.15, σ_c=40kg/cm^2, σ_t=10kg/cm^2

The density was taken equal to 2.4g/cm^3 in all cases. A quasi-static study was performed for a constant value of the PCB parameter $\beta = 0.9$.

Figure 14 shows the evolution of the global damage index for increasing values of the self weight. Convergence of the solution was lost for D=0.84 and a safety coefficient of 5.75 was found. The contours of equal displacement at that load level are displayed in Figure 15 whereas the damage

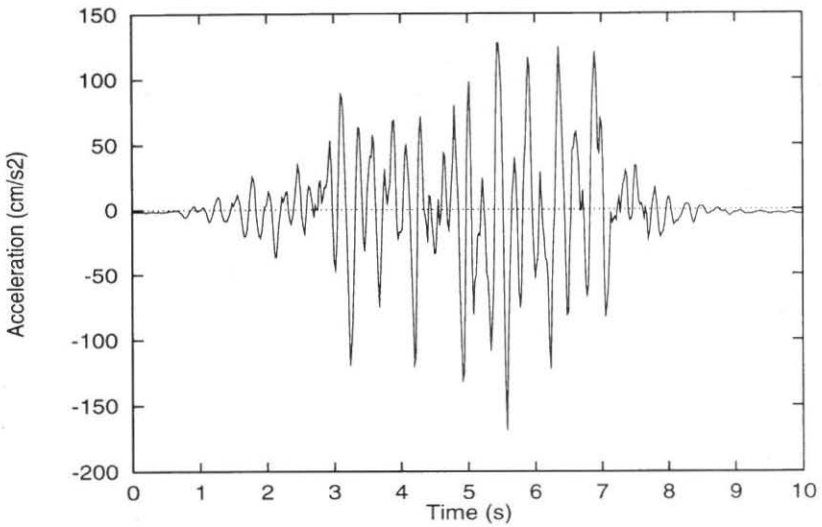

Figure 9. Synthetic accelerogram.

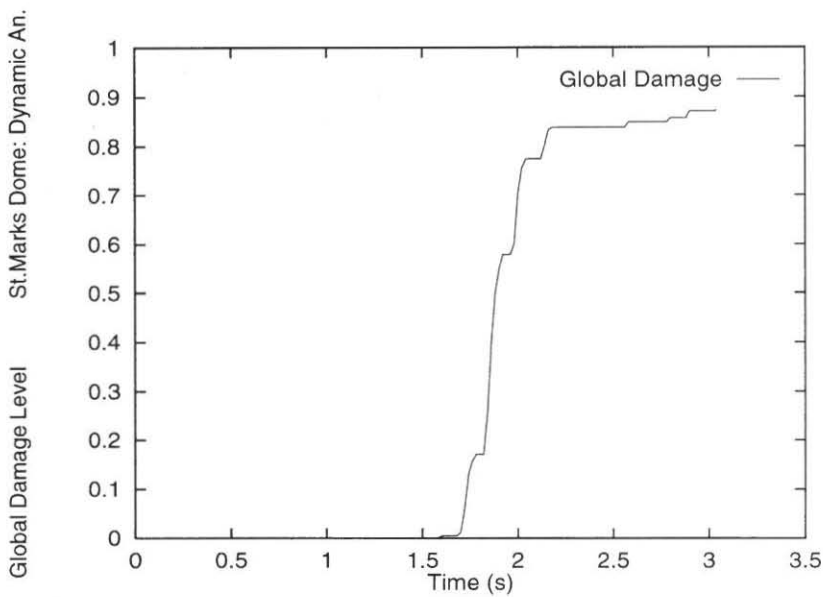

Figure 10. Global damage evolution for the dynamic analysis.

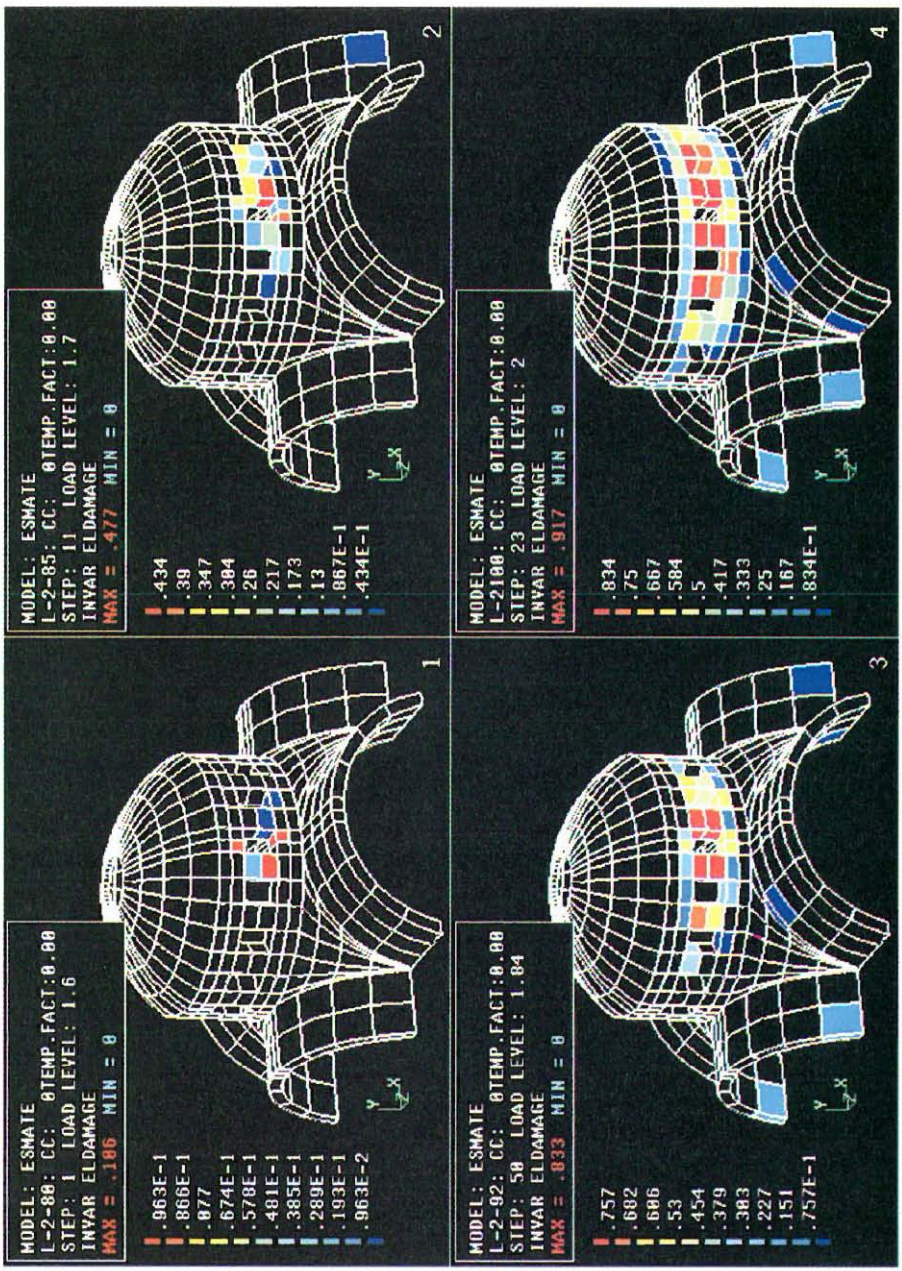

Figure 11.a Contours of the damaged zones during the dynamic loading history, corresponding to the triggering of the damage process, for the time instants of 1.6,1.7,1.84 and 2.0 seconds.

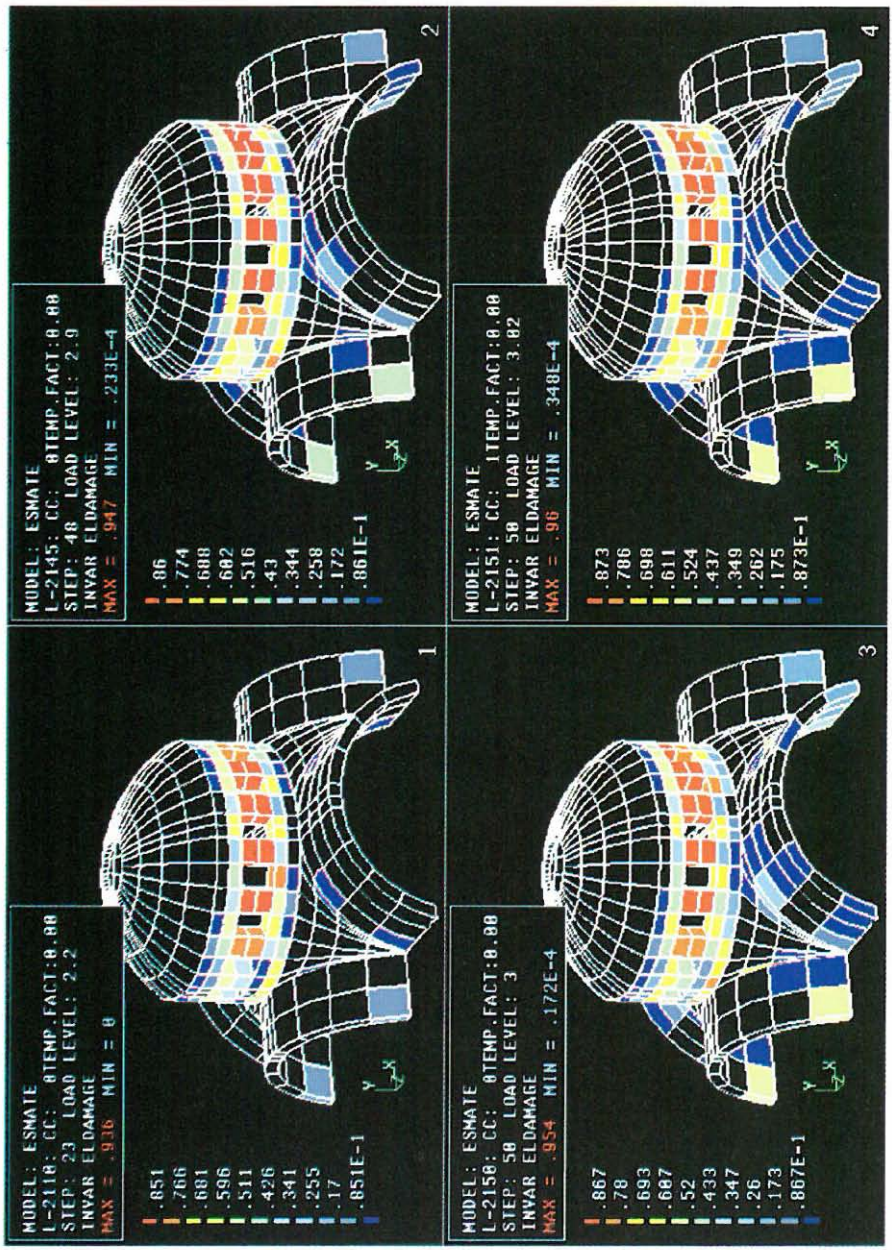

Figure 11.b Contours of the damaged zones during the dynamic loading history, corresponding to the final stages before structural collapse, for the time instants of 2.2, 2.9, 3.0 and 3.02 seconds.

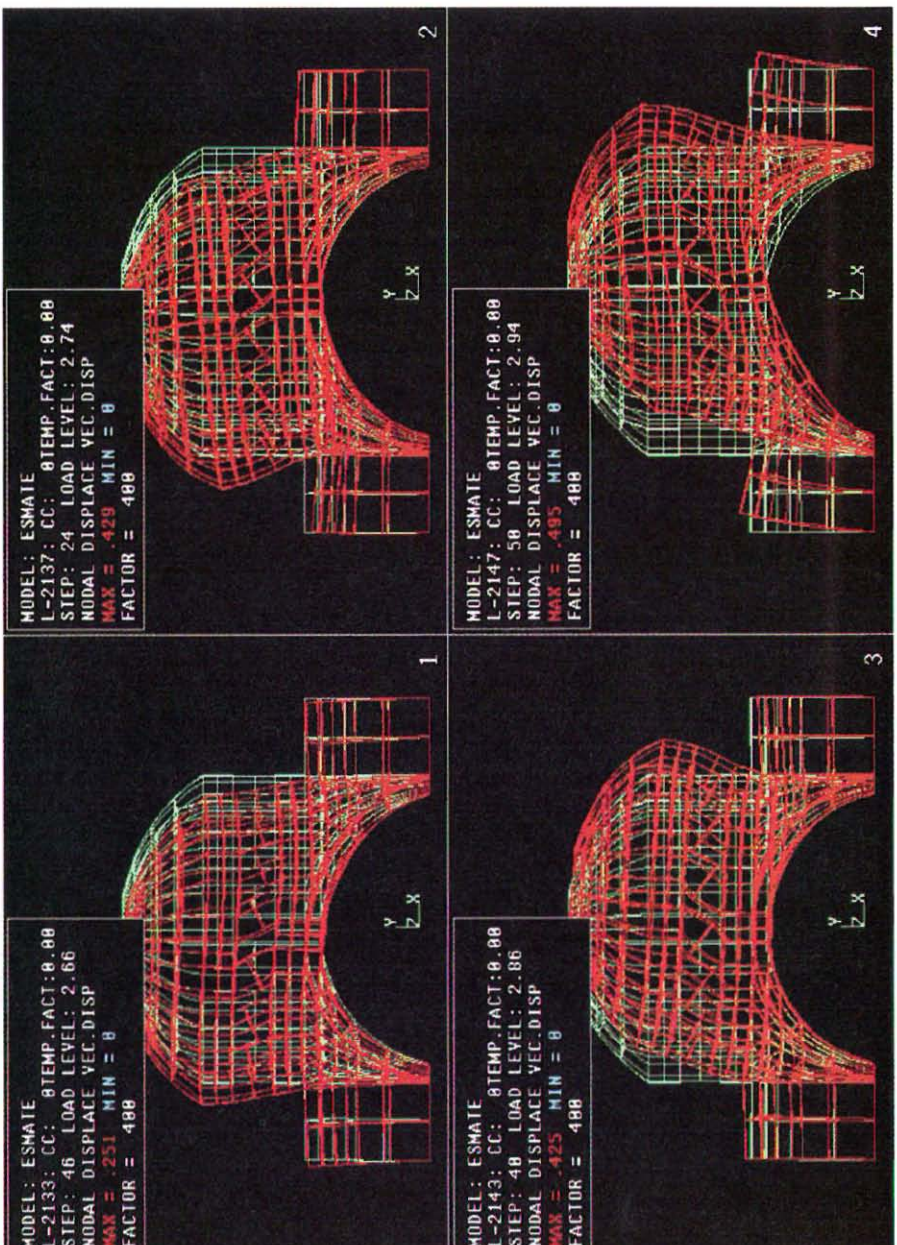

Figure 12. Deformed shapes corresponding to the vibration of the structure immediately before collapse.

Figure 13. Finite Element mesh for the full 3D analysis of the 5 domes.

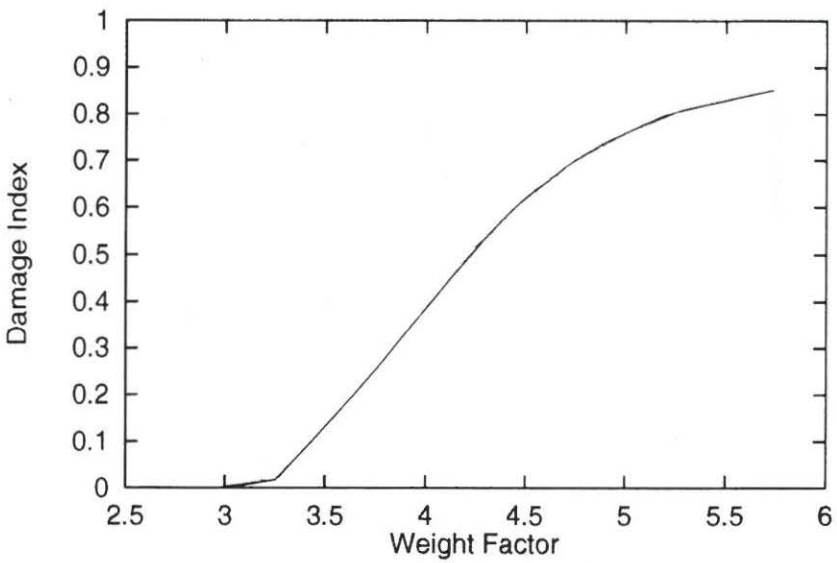

Figure 14. Evolution of global damage function of the self-weight factor.

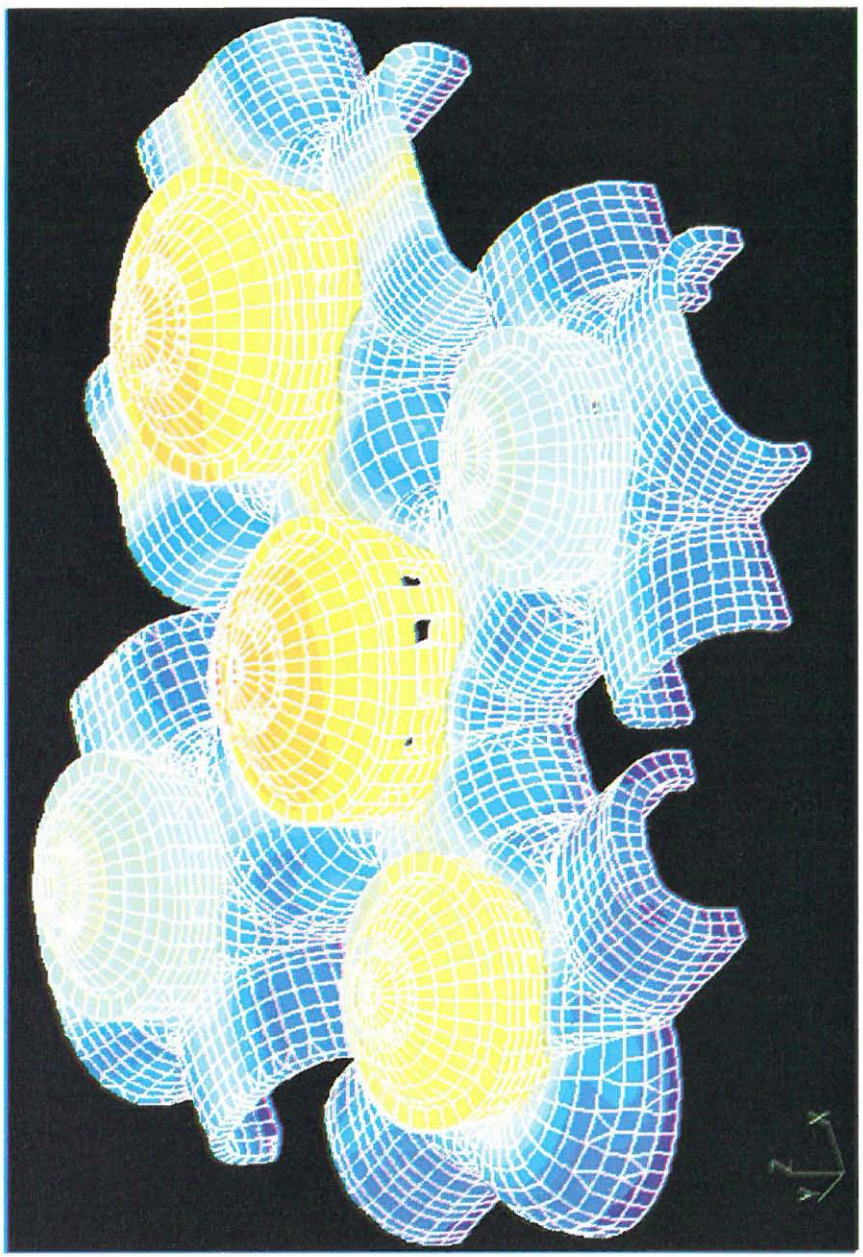

Figure 15. Contours of equal displacement for a 5.75 self-weight factor.

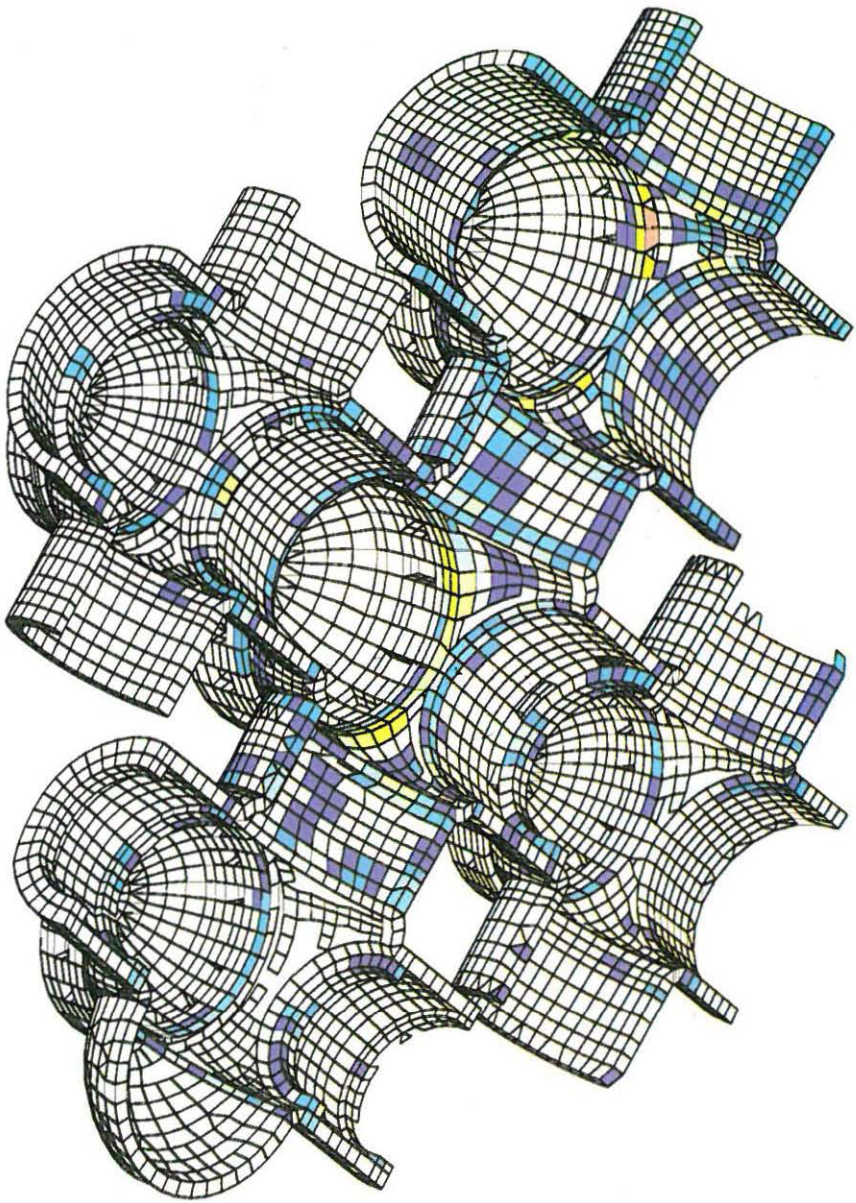

Figure 16. Damage contours for a 5.75 self-weight factor.

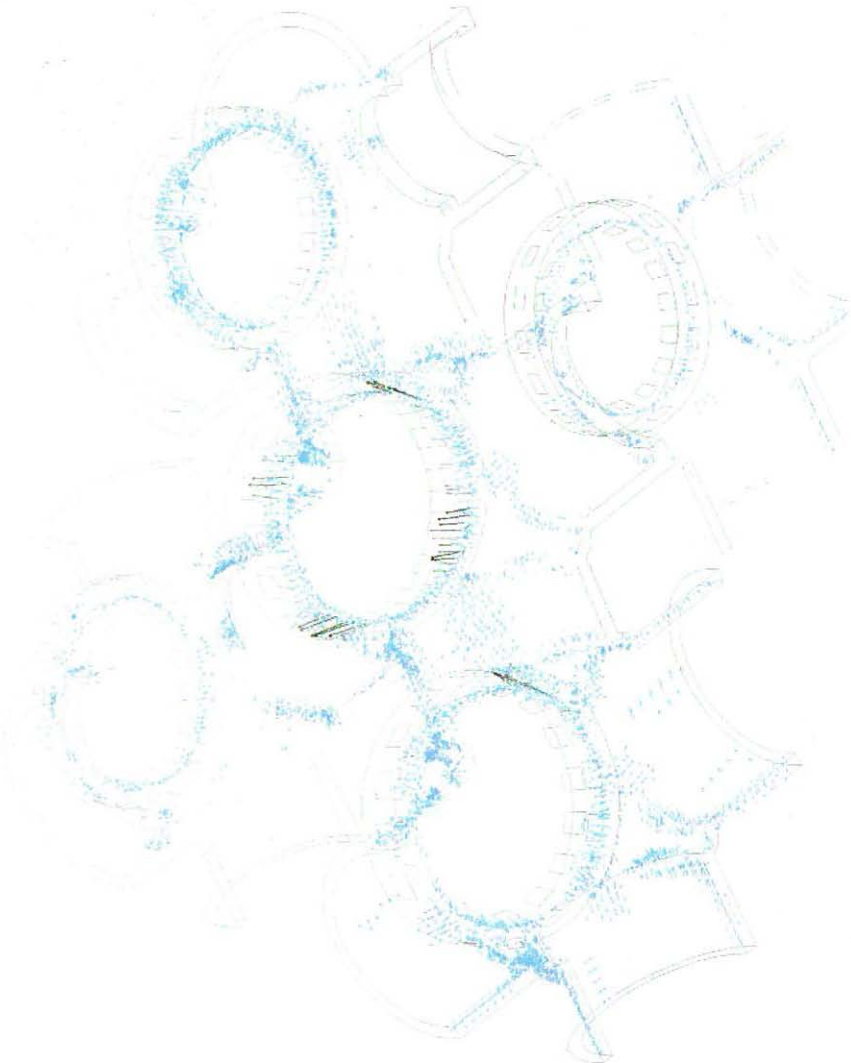

Figure 17. Crack patterns for a 5.75 self-weight factor.

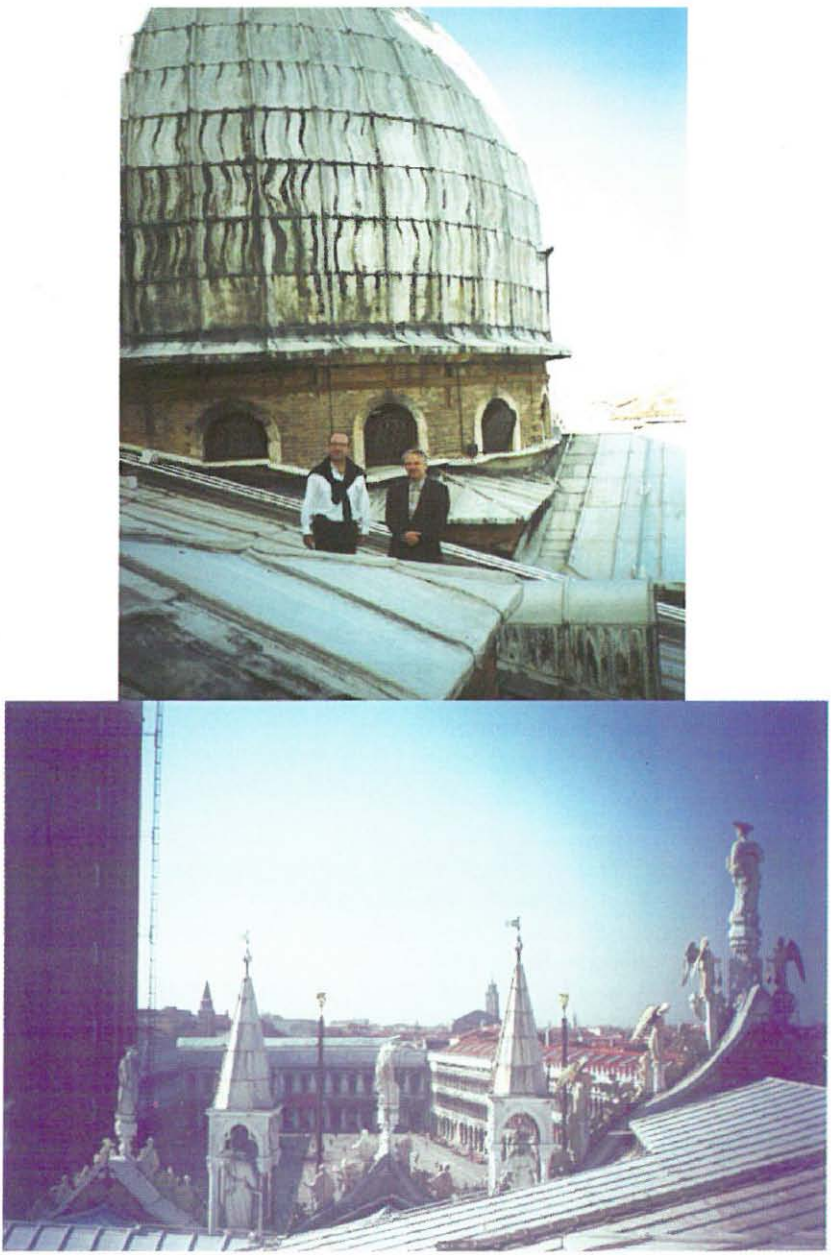

Figure 18. Above: The central dome of St. Mark's Basilica.
Below: Perspective of St. Mark's square from the roof.

contours are shown in Figure 16.

Figure 17 shows finally the crack pattern at failure. Cracks have been assumed to appear at each integration point in the orthogonal direction to the maximum principal strain. The size of each crack has been defined as proportional to the damage level at that point. Figure 17 shows that failure occur due to accumulated damage at the base of the masonry walls and at the central stone arches.

Figure 18 shows finally a close-up picture of the central dome taken during a recent visit of the first author to St. Marks Basilica in the company of the architect responsible for its maintenance Mr. E. Vio. A perspective of St. Marks square taken from the Basilica's roof is also shown in the second photograph.

7. CONCLUDING REMARKS

The environmental-mechanical damage methodology presented can be applied successfully to assess the structural conditions and estimate the safety level and durability of historical constructions under static and dynamic loading. A full coupled solution taking into account physical-chemical-biological degradation and mechanical effects is nowadays possible and this will allow to trace the history of structural pathologies and to design the correct intervention measures. A particularly interesting immediate application of the damage model here proposed is the evaluation of *the structural strength increase* for different intervention measures, thus allowing to optimize any restoration investment.

REFERENCES

[1] ENCO (ed). *Materiali negli Edifici Storici: Degrado e Restauro*, by Collepardi, M., Coppola, L., Spresiano 1990

[2] IABSE (ed). *Structural Preservation of the Architectural Heritage*, IABSE Symposium, Rome 1993

[3] Brebbia, C.A. and Leftheris, B. (Eds.) "*Structural Studies of Historical Buildings*" Comput. Mech. Publication 1995

[4] Collepardi, M. Degradation and restoration of masonry walls of historical buildings, *Material and Structures*, 1990, **23**, 81-102.

[5] Oñate, E. Reliability analysis of concrete structures. Numerical and experimental studies, *Evoluzione nella sperimentazione per le costruzioni*, pp. 125-146, Seminar CISM, Merano, April 1994.

[6] Bazant, Z., "Mechanics of distributed cracking", *Appl. Mech. Rev.*, Vol. **39**, pp. 676-705, 1986

[7] ASCE Committee on Concrete and Masonry Structures, Task Committee on Finite Element Analysis of Reinforced Concrete Structures: A State-of-The-Art Report on Finite Element Analysis of Reinforced Concrete Structures, *ASCE Spec. Pub.*, 1981

[8] Wastiels, J., "Behaviour of concrete under multi-axial stresses a review", *Cement and Concrete Research*, Vol. **9**, pp. 35-44, 1979

[9] Kupfer, H.B. and Gerstle, K.K., "Behaviour of concrete under biaxial stresses", *ASCE Journal of the Eng. Mech. Div.*, Vol. **99**, N^o **EM4**, pp. 853-866, 1973

[10] Oller, S., "Modelización numérica de materiales friccionales", Monograph CIMNE, 1991

[11] Mang, H., Bićanić, N. and de Borst, R. (Eds.), "*Computer modeling of concrete structures*", Proc. EURO-C, Innsbruck, Austria, 1994

[12] Oñate, E., Oller, S., Oliver, J. and Lubliner, J., "A constitutive model for cracking of concrete based on the incremental theory of plasticity", *Engng. Comput.*, **5**, 309-20, 1988

[13] Lubliner, L., Oller, S., Oliver, J. and Oñate, E., "A plastic damage model for nonlinear analysis of concrete", *Int. J. Solid Struct.*, Vol. **25**, 3, pp. 299-326, 1989

[14] Barbat, A.H., Oller, S., Oñate, E. and Hanganu, A., "Simulation of damage phenomena in required concrete buildings subjected to seismic actions", *Numerical Methods in Engn. and Applied Sciences*, H. Alder et al. (Eds.), CIMNE, Barcelona 1992

[15] Hanganu, A., Oller, S., Oñate, E. and Barbat, A.H., "A finite element model for damage analysis of nuclear reactor containment shells", *2d National Conference on Boundary and Finite Element*, Sibiu, Romania, May, 13-15, 1993

[16] Cervera, M., Oliver, J., Herrero, E. and Oñate, E., "A computational model for progressive cracking in large dams due to swelling of concrete", *Engng. Fracture Mechanics*, **35**, No. 1, 2, 3, pp. 575-85, 1990.

[17] Lemaitre, J., "A Continuous Damage Mechanics Model for Ductile Fracture", *Journal Engng. Mater. Tech.*, Vol. **107**, pp. 83-89, 1985.

[18] Lemaitre, J., "How to use Damage Mechanics", *Nuclear Engineering and Design*, No. **80**, pp. 233-245, 1984

[19] Simó, J.C. and Ju, J.W., "Strain and Stress Based Continuum Damage Models-I. Formulation", *International Journal Solids & Structures*, Vol. **23**, pp. 821-840, 1987.

[20] Simó, J.C. and Ju, J.W., "Strain and Stress Based Continuum Damage Models-II. Computational Aspects", *International Journal Solids & Structures*, Vol. **23**, pp. 841-869, 1987.

[21] Kachanov, L.M., "Continuum Model of Medium with Cracks", *Journal of the Engineering Mechanics Division*, ASCE, Vol. **106**, No. EM5, pp.

1039-1051, 1980.

[22] Faria, R. and Oliver, J., "A rate dependent plastic-damage constitutive model for large scale computation in concrete structures" *Monograph CIMNE* No. **17**, Barcelona, January 1993.

[23] Oliver, J. Cervera, M., Oller, S. and Lubliner, J., "Isotropic damage models and smeared crack analysis of concrete". Proc. 2d Int. Conf. on Comp. Aided Analysis of Concrete Struct., Zell am See, Austria, pp. 445-57, N. Bicanic et al. (Eds.), Balkema 1990.

[24] Oñate, E., Oliver, J. and Bugeda, G., "Finite element analysis of nonlinear response of concrete dams subject to internal loads., "Europe-US Symposium on Finite Element Methods for Nonlinear Problems, (Edited by Bergan, Bathe and Wunderlich) Springer Verlag, 1986.

[25] Arrea, M. and Ingraffea, A.R., "Mixed mode crack propagation in mortar and concrete", *Cornell Univ., Dept. Struct. Engng. Report 81-13*, Ithaka, New York, 1981.

[26] Cervera, M., Oliver, J. and Galindo, M., "*Simulación Numérica de Patologías en Presas de Hormigón*", Monografía CIMNE no. **4**, Barcelona, June 1991.

[27] Cervera, M., Oliver, J. and Galindo, M.,"Numerical Analysis of Dams with Extensive Cracking Resulting from Concrete Hydration: simulation of a real case", *Dam Engineering*, Vol. **3**, Issue 1, 1992.

[28] Hanganu, A., "Análisis Dinámico No Lineal de Estructuras de Hormigón Armado con Modelos de Daño", Ph.D. Thesis, in development.

[29] Saetta, A., Schrefler, B., Vitaliani, R. "The carbonation of concrete and the mechanism of moisture, heat and carbon dioxide flow through porous materials, *Cem. and Conc. Res.*, 1993, **23**, 761-772.

[30] Saetta, A., Scotta, R., Vialiani, R. "The numerical analysis of chloride penetration in concrete, *ACI Mat. Jour.*, 1993, **90**, 441-451.

[31] Creazza, G. Structural Behaviour of San Marco Basilica, Venice IABSE SEI Volume, 3 Number 1, February 1993.

[32] Collepardi, M., Coppola L., Monosi, S. Chemical attack of calcium chloride on the Portland cement paste, *il Cemento*, 1989, 2, 97-104.

[33] Schefler, B.D., "Finite elements in environmental engineering: complete thermo-hydro-mechanical processes in porous media including pollutant transport",*Archives of Computational Methods in Engineering*, **2**, 3, 1-55, 1995

[34] Creazza, G., Saetta, A., Scotta, R., Vitaliani. R. and Oñate, E., "Mathematical simulations of structural damage in historical buildings", *Structural Studies of Historical Buildings IV*, C.A. Brebbia and B. Leftheris (Eds.), Vol. 1 , pp. 111, 1995

[35] Ziekiewicz, O.C. and Taylor, R.L., "The Finite Element Method", McGraw Hill, Vol. 1, 1989, Vol. 2, 1991.